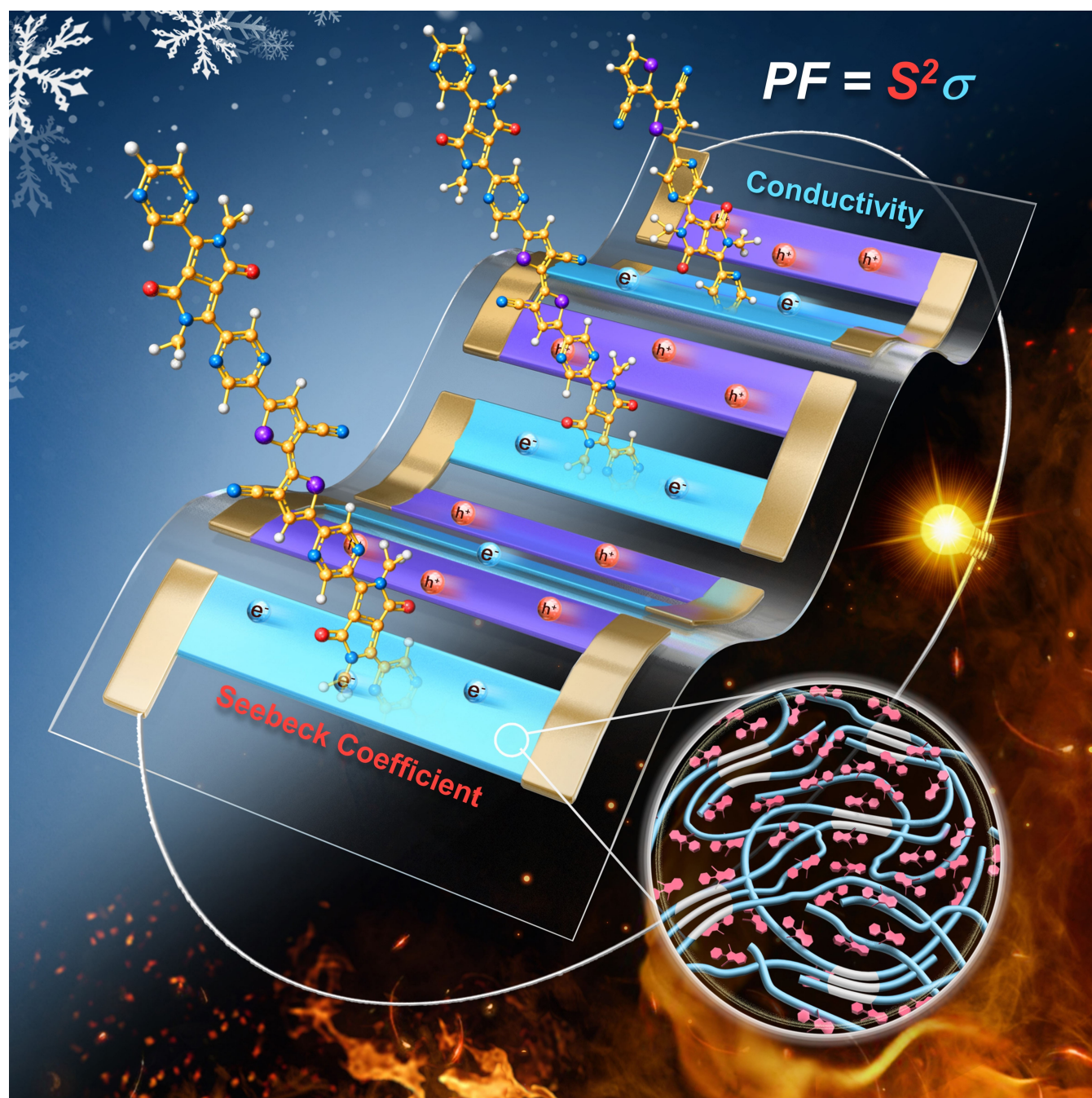


Special  
Collection

# Recent Progress on Addressing the Key Challenges in Organic Thermoelectrics

Jia-Tong Li and Ting Lei<sup>\*[a]</sup>

**Abstract:** Compared with inorganic thermoelectric materials, organic thermoelectric (OTE) materials have attracted increasing attention due to their advantages of low toxicity, high mechanical flexibility, and large-scale solution processability. In the past few years, OTE materials have made remarkable progress in terms of their design, synthesis, and device performance. However, some challenges remain, including the low doping efficiency in n-type materials, poor doping

stability with molecular dopants, and the largely reduced Seebeck coefficient after heavily doping, *etc.* All these factors hinder the further development of OTEs for commercial applications. In this Minireview, we highlight several key challenges during the development of OTEs and summarize recent understandings and efforts to address these challenges.

## 1. Introduction

To date, the best thermoelectric materials are based on inorganic compounds (e.g.  $\text{Bi}_2\text{Te}_3$ ), which usually contain low Earth abundance or toxic elements and require complex high temperature and high vacuum processing routes.<sup>[1]</sup> Recently, organic thermoelectrics (OTEs) have attracted ever-increasing attention because OTEs have shown figure-of-merit approaching those of the inorganic materials at low-temperature range ( $< 200^\circ\text{C}$ ), while keeping good large-area processability and high mechanical flexibility.<sup>[2]</sup> The thermoelectric performance of a material is generally evaluated by the dimensionless figure of merit,  $ZT$ ,

$$ZT = \frac{S^2\sigma}{\kappa} T \quad (1)$$

where  $T$  is the absolute temperature,  $S$  is the Seebeck coefficient,  $\sigma$  is the electrical conductivity, and  $\kappa$  is the thermal conductivity. Organic semiconductors (OSCs) usually have low thermal conductivities ( $< 0.3 \text{ W/mK}$ ),<sup>[3]</sup> since they form solids through van der Waals interactions with poor lattice thermal conductivity. Hence power factor ( $PF = S^2\sigma$ ) is often used for evaluating the performance of an OTE material. Besides, to realize a high-performance thermoelectric device, both p- and n-type OTEs with comparable performance are required.<sup>[4]</sup> To date, p-type conjugated polymer PEDOT: PSS has shown high conductivities over  $100 \text{ S cm}^{-1}$  and  $ZT$  values over 0.4,<sup>[2a]</sup> and n-type small molecule A-DCV-DPPTT<sup>[5]</sup> can achieve conductivities over  $5 \text{ S cm}^{-1}$  and  $ZT$  values over 0.2 at low-temperature range (Figure 1). For commercial applications,  $ZT$  values over 1 with good stability are expected. Therefore, further enhancing the thermoelectric performance (both  $\sigma$  and  $S$ ) of organic semiconductors are essential.

The electrical conductivity of a material is determined by its carrier charge  $q$ , electron mobility  $\mu$ , and charge carrier concentration  $n$ :  $\sigma = qn\mu$ . OSCs usually have low charge carrier


density and thereby low conductivities, both of which can be effectively enhanced via chemical doping. However, the efficiency and stability of doping are always unsatisfactory. Low doping efficiency is often due to the mismatch of the energy level and the poor miscibility between the OTE materials and dopants.<sup>[6]</sup> After doping, de-doping caused by dopants diffusion and evaporation can also decrease the electrical conductivities.<sup>[7]</sup> Hence, improving both doping efficiency and doping stability is a key issue to achieve good electronic performances of OSCs.<sup>[8]</sup> For all types of thermoelectric materials, the Seebeck coefficient always shows an inverse relationship with charge carrier density, while the Seebeck coefficient of organic materials decreases significantly after heavily doping,<sup>[2b]</sup> which, to date, is poorly understood and still under debate.

In this Minireview, we highlight several key challenges in the development of OTEs and summarize recent progress on addressing the challenges. For enhancing the electrical conductivity ( $\sigma$ ), we focus on analyzing factors that may influence the doping efficiency and doping stability, including energy level mismatch, miscibility, counterion effects, and dopant diffusion issues. As for the Seebeck coefficient ( $S$ ), we try to present recent understandings on charge transport mechanisms, doping-induced structural and energetic disorders, and their effects on  $S$ . The aim of this review is to provide chemists some basic knowledge of OTE materials, as well as some material design strategies and device optimization approaches for high-performance OTE materials.

## 2. Conductivity enhancement by doping

Doping organic semiconductors can be realized by field-effect gating, electrochemically ion injection, and chemical doping (Figure 2). Field-induced doping often used in field-effect transistor (FET) configuration can provide low to moderate charge carrier concentrations ( $10^{17}$ – $10^{19} \text{ cm}^{-3}$ ) near the dielectric surface. FET has been used to understand the intrinsic Seebeck coefficients of conjugated polymer without counterion interference on the charge transport properties.<sup>[9]</sup> Ion-gel based electrochemical doping, also using a FET device configuration, can provide tunable and high charge carrier concentrations through ion injection ( $> 10^{20} \text{ cm}^{-3}$ ), e.g. 0.2 holes per monomer for P3HT,<sup>[10]</sup> and is a good approach to understand the charge transport properties in heavily doped OTEs.<sup>[11]</sup> Chemical doping using a redox reagent can provide low to extremely high

[a] J.-T. Li, Prof. T. Lei  
Key Laboratory of Polymer Chemistry and  
Physics of Ministry of Education  
School of Materials Science and Engineering,  
Peking University  
Beijing 100871 (P. R. China)  
E-mail: tinglei@pku.edu.cn

 This manuscript is part of a special collection dedicated to Early Career Researchers.

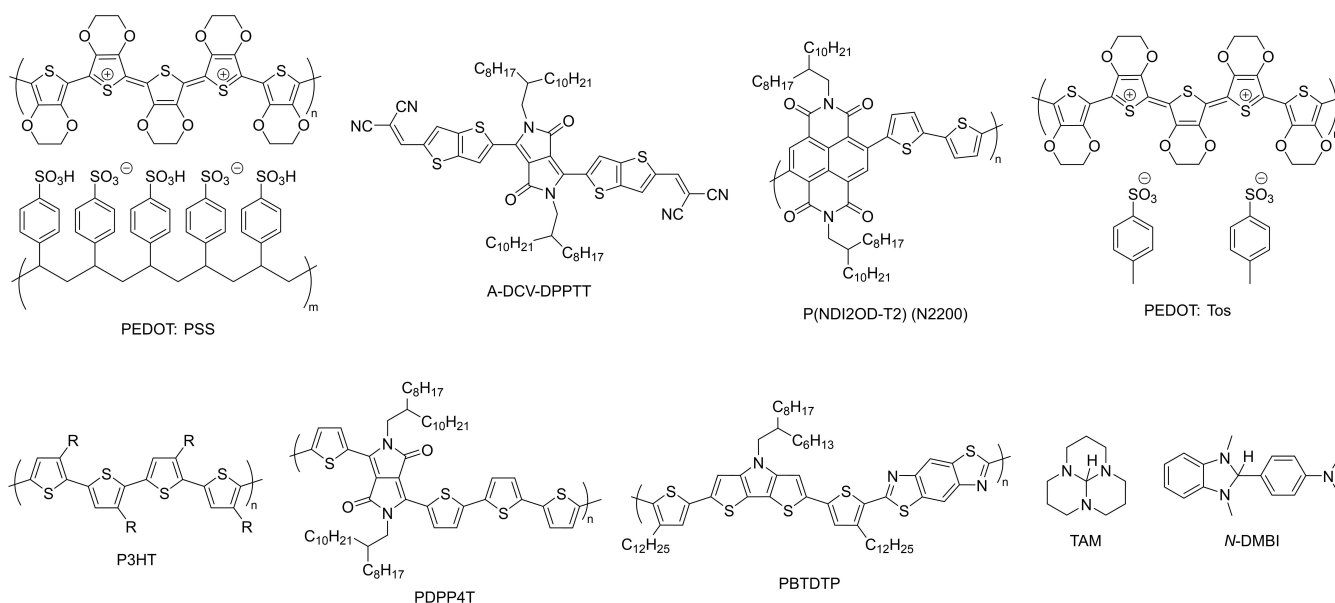


Figure 1. Chemical structures of some OTE materials and dopants discussed in this Review.

doping concentrations by controlling the dopant/OSC ratio. It does not need any specific device structure, and is the most widely used method in doping OTE materials. Chemical doping can be performed by direct polymer/dopant mixing or by sequential doping (Figure 2c). Direct mixing is performed by blending dopant and polymer in solution and then depositing polymer and dopant on substrate. This method allows better chemical reactions but may largely affect the OSC film morphology. In contrast, sequential doping can sustain the

morphology of the pre-casted high-quality host film via subsequent immersion, spin-coating, or vapor deposition to introduce dopants.<sup>[12]</sup> In these chemical doping methods, doping efficiency, counterion effects, and doping stability play important roles to influence the electrical conductivity. (Figure 3).

## 2.1. Energy level

To achieve high doping efficiency, OSCs and dopants with appropriate energy level offset are usually expected, i.e. for p-doping, the dopant's LUMO energy level should be lower than the HOMO energy level of the OSC, while for n-type doping, the dopant's HOMO energy level should be higher than the LUMO energy level of the OSC. However, in many cases, the unfavorable offset between dopant and OSCs for charge transfer can also provide good doping efficiency and TE performance.<sup>[13]</sup> This could be attributed to (1) the energy deficit for charge transfer can be compensated for by the Coulomb interaction between the ionized dopants and polarons on the OSCs;<sup>[14]</sup> (2) the partial charge transfer between dopants and OSCs;<sup>[15]</sup> (3) chemical reactions between dopants and OSCs, e.g. proton transfer in p-doping<sup>[16]</sup> or hydride transfer in n-doping.<sup>[17]</sup>

P-type dopants are abundant, containing small-size inorganic oxidants (e.g.  $\text{FeCl}_3$ ) or Lewis acid (e.g.  $\text{BF}_3$ ), small molecules (e.g.  $\text{F}_4\text{TCNQ}$ ), and polymers (e.g. PSS). These p-type dopants are strong oxidants or acids and can strongly p-dope OSCs without significantly disrupting the molecular packing, yielding high electrical conductivities. To date, p-doped OSCs, especially thiophene-based polymers, can be doped with high hole concentrations over  $10^{21} \text{ cm}^{-3}$  and have exhibited high electrical conductivities over  $1000 \text{ S cm}^{-1}$  ( $> 5000 \text{ S cm}^{-1}$  for PEDOT:PSS;<sup>[18]</sup>  $> 1000 \text{ S cm}^{-1}$  of PBTTT).<sup>[19]</sup> However, only a few

Jia-Tong Li is a Ph.D. student in School of Materials Science & Engineering, Peking University. He obtained B.E. in School of Materials Science and Engineering from Peking University in 2019. His current research focuses on polymer semiconducting materials, organic thin-film transistors and organic thermoelectrics.



Ting Lei is an assistant professor in School of Materials Science & Engineering, Peking University. He received B.S. and Ph.D. from Peking University in 2008 and 2013. After a postdoc training at Stanford University, he joined Peking University in 2018. His current researches focus on organic/polymer functional materials, organic electronics, carbon-based electronics, and bioelectronics.



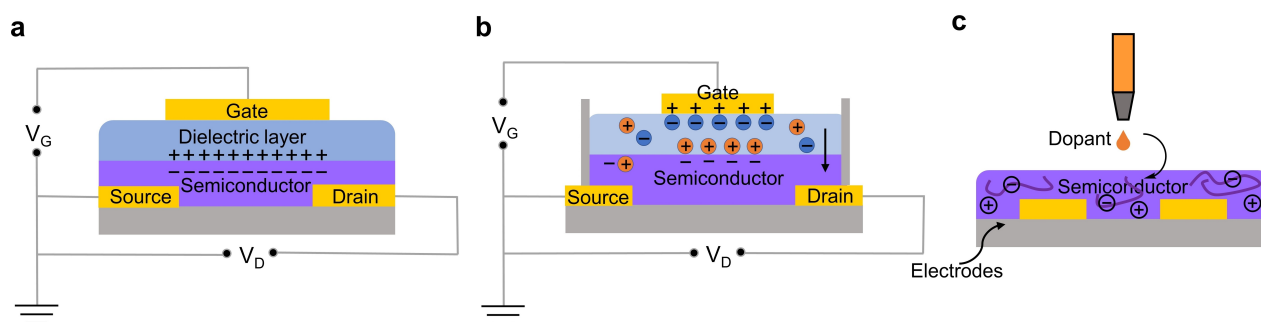


**Figure 2.** Schematic illustration of a electrical field-induced doping using a field-effect transistor device configuration; b ion gel based electrochemical doping by ion injection; c chemical doping process via sequential casting.

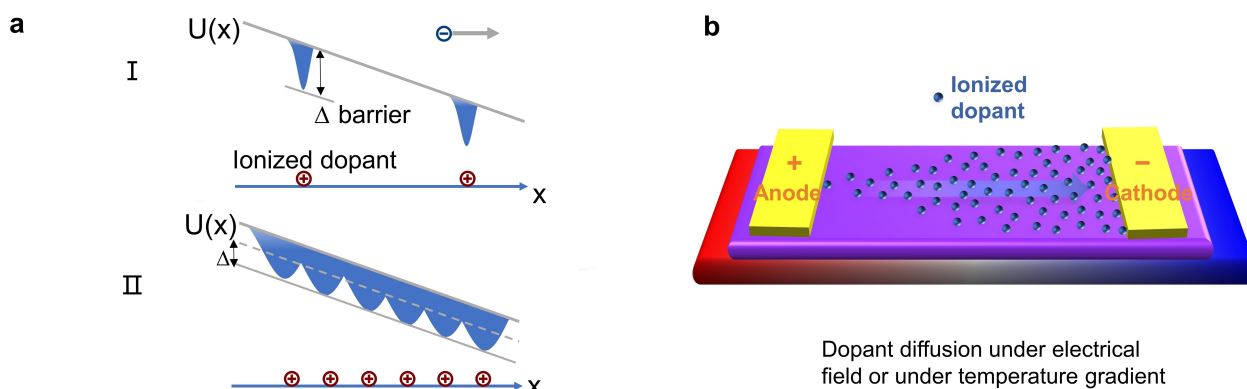


**Figure 3.** a) Counterion effect with Coulomb traps according to the different doping levels: (1) steep transport barrier at low doping level; (3) flat transport barrier at high doping level where  $U(x)$  is the electrostatic potential for carriers. b) Ionized dopant diffusion for dopant anions in the n-type doping system caused by electrical field biasing and temperature gradient.

n-doped conjugated polymers demonstrated conductivities over  $10 \text{ Scm}^{-1}$ .<sup>[4]</sup> This is probably due to the weak reducing ability and the large size of most n-type dopants. To achieve good air-stability for n-dopants, they usually have limited reducing ability, thus preventing their n-doping ability.

Designing suitable n-dopants is challenging since it requires high reducing ability, good air stability, and adequate miscibility with OSCs.<sup>[17]</sup> Furthermore, the n-doped OSCs also face air stability issues due to high-lying LUMO energy levels after doping. Thus, lowering the LUMO energy level of n-type OSCs is an effective strategy to enhance both n-doping efficiency and the OTE materials' stability.<sup>[8,20]</sup> Polymers with low LUMO energy levels are less, and developing electron-deficient n-type conjugated polymers is highly desired. Diketopyrrolopyrrole (DPP) based polymers have shown high mobilities in FETs,<sup>[21]</sup> nevertheless, their performances in n-type OTEs still lag far behind those of their p-type counterparts.<sup>[22]</sup> To address this issue, our group designed and synthesized a new diketopyrrolopyrrole (DPP) derivative, pyrazine-flanked DPP (PzDPP), which displays the deepest LUMO level among all DPP building blocks (Figure 4a).<sup>[23]</sup>

Since several studies have suggested that electron-deficient modification of the donor moiety can enhance the electron affinity of the D–A polymers,<sup>[4a,22]</sup> we employed an electron-deficient “donor”, 3,3'-dicyano-2,2'-bithiophene to further lower the LUMO energy level of the polymer. The polymer, P(PzDPP-

CT2) showed better planarity and stronger electron affinity compared to a reference polymer thiophene-flanked DPP polymer, P(TDPP-CT2). When doped with a commonly used dopant *N*-DMBI, P(PzDPP-CT2) film showed higher doping level as demonstrated by the absorption spectra and other characterization methods. The higher n-doping efficiency endows P(PzDPP-CT2) film with high n-type conductivities of up to  $8.4 \text{ Scm}^{-1}$ , much higher than that of the reference polymer ( $0.39 \text{ Scm}^{-1}$ ). The polymer also exhibited a high *PF* value of  $57.3 \mu\text{Wm}^{-1}\text{K}^{-2}$ , which is among the highest in solution-processed n-doped conjugated polymers. For n-type OTE materials, lowering LUMO energy level is an effective strategy, which has been widely employed recently.<sup>[24]</sup>

## 2.2. Miscibility issue

Miscibility is another key factor that strongly influences the doping efficiency. For a typical doping process, only when the dopant and OSC have close contact, the doping, either electron or proton/hydride transfer, can happen,<sup>[25]</sup> which requires the small-molecule dopants to insert into the molecular packing of OSCs. This process is not trivial and requires good miscibility, otherwise, the dopant and OSC would form separated phase and hinder the transport of carrier charges. Recently, several molecular design strategies to enhance the miscibility have

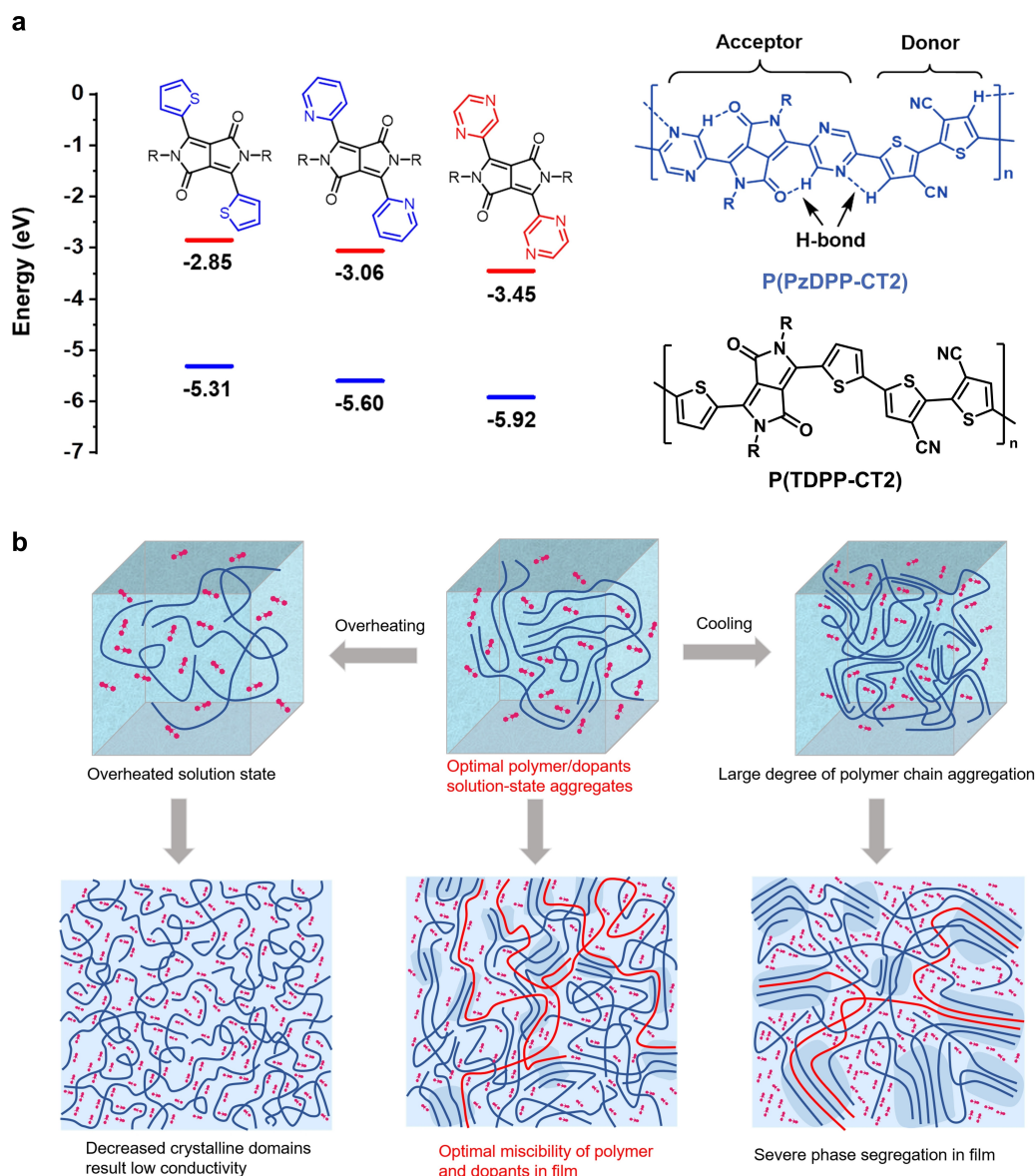


**Figure 4.** a) Energy level comparison for several DPP building blocks and molecular structures the D–A polymers P(PzDPP-CT2) and P(TDPP-CT2). Adapted with permission from Ref. 38. Copyright 2019 American Chemical Society. b) Strategy on controlling the solution-state P(PzDPP-CT2) aggregates at 1-CN to achieve the optimal microstructures and miscibility with dopants in the solid state. Adapted with permission from Ref. 38. Copyright 2021 Wiley-VCH Verlag GmbH & Co.

been reported, such as the introduction of polar ethylene glycol (EG) side chains,<sup>[26]</sup> using twisted polymer building block<sup>[27]</sup> and “kinked” donor moieties.<sup>[6]</sup> Polar groups, such as ethylene glycol side chains, can interact with the ionized counterions and allow the counterions to be uniformly distributed in the polymer matrix. “Twisted” or “kinked” polymer building blocks reduce the strong  $\pi$ - $\pi$  interactions in high-mobility conjugated polymers and contribute to efficient diffusion of dopants into the polymer matrix, achieving higher doping efficiency. However, these molecular design strategies always result in disordered molecular packing (EG chains vs. alkyl chains) and poor interchain interactions (“twisted” or “kinked” vs. planar), thus leading to significantly decreased charge carrier mobilities and finally low electrical conductivities. To overcome these limita-

tions, our group recently reported a general approach to enhance the miscibility and doping efficiency in conjugated polymers without modifying molecular structures.<sup>[28]</sup> Because of the strong interchain interactions in high-mobility conjugated polymers, many studies have reported that conjugated polymers tend to aggregate even in dilute solutions.<sup>[29]</sup> Using P(PzDPP-CT2) as an example, we found that the polymer aggregation behavior in solution has a profound influence on the dopant-polymer miscibility (Figure 4b). P(PzDPP-CT2) strongly aggregated in poor solvents (e.g. *p*-xylene) even at high temperatures. In a good solvent 1-chloronaphthalene (CN), the polymer can be fully disaggregated at 200 °C. More importantly, conjugated polymers have slow dynamics after being disaggregated. These features allow us to modulate the

polymer aggregates by tuning the processing solvents, temperatures, and aging time. After carefully tuning the polymer aggregates in solution, the polymer-dopant miscibility and doping efficiency in solid-state can be greatly enhanced. The disaggregated P(PzDPP-CT2) polymer exhibited one order of magnitude higher conductivities of up to  $32.1 \text{ Scm}^{-1}$ , much higher than the strongly aggregated polymer solutions (e.g., in *p*-xylene,  $2.6 \text{ Scm}^{-1}$ ). Using the same strategy, the electrical conductivity of a widely studied n-type polymer N2200 was also doubled, suggesting that our method could be general for different types of conjugated polymers.

Apart from engineering polymer structures and processing conditions, developing highly miscible n-type dopants is also an effective approach. The most commonly used n-type dopants are *N*-DMBI. However, other *N*-alkyl substituted 1*H*-benzimidazoles were also developed.<sup>[30]</sup> Different alkyl substituents on *N*-DMBI influence the dopant intercalation into the polymer matrix, and longer alkyl substituents could enhance the miscibility between dopant and polymer. Recently, Pei and coworkers reported a new triaminomethane type n-dopant, TAM (Figure 1), which has an alkyl-substituted guanidine structure.<sup>[17]</sup> The counterion of TAM exhibited good miscibility with the polymer alkyl side chains and can form uniform doping in polymer matrix without significantly disturbing the polymer packing in solid state. TAM has a thermally activated doping mechanism, and thus it is very stable at ambient conditions but highly active after being heated. By using TAM as the dopant, a high electrical conductivity over  $21 \text{ Scm}^{-1}$  and a *PF* over

$51 \mu\text{Wm}^{-1} \text{K}^{-2}$  were achieved in a thick polymer film ( $> 10 \mu\text{m}$ ). The *PF* values are much higher than the commonly used *N*-DMBI dopant, suggesting a great potential of developing new dopants to enhance n-doping efficiency.

### 2.3. Counterion effect

After doping, there exists various charged species including polaron, bipolaron and ionized dopants in the doped film. Those ionized dopants attract the carrier with the Coulombic interaction and exhibit the counterion effect.<sup>[31]</sup> At low doping level, separated counterions form the steep Coulomb traps which suppress the mobility. At higher doping level, the Coulomb traps overlap and decrease the charge transport barrier (Figure 3a). Due to the influence of transport barrier, the counterion effect indeed restrict the delocalization of free charged carriers. Yamashita *et al.*<sup>[32]</sup> recently reported an 'anion exchange' approach to overcome the theoretical doping limitation and reduce the Coulomb interaction between charge carriers and ionized dopant (Figure 5a). After doping, the p-type polymer (PBTTT) is oxidized to form polaron or bipolaron, and the dopant (F4TCNQ) is reduced to F4TCNQ radical anion. By immersing in proper ionic liquids, stable and effective anion exchange can happen, and the F4TCNQ<sup>-</sup> can be replaced by different sizes of the anions (Y<sup>-</sup>) from the ionic liquid. The gain of the Gibbs free energy is considered as the main driving force in the anion exchange process, influenced by the size of cations

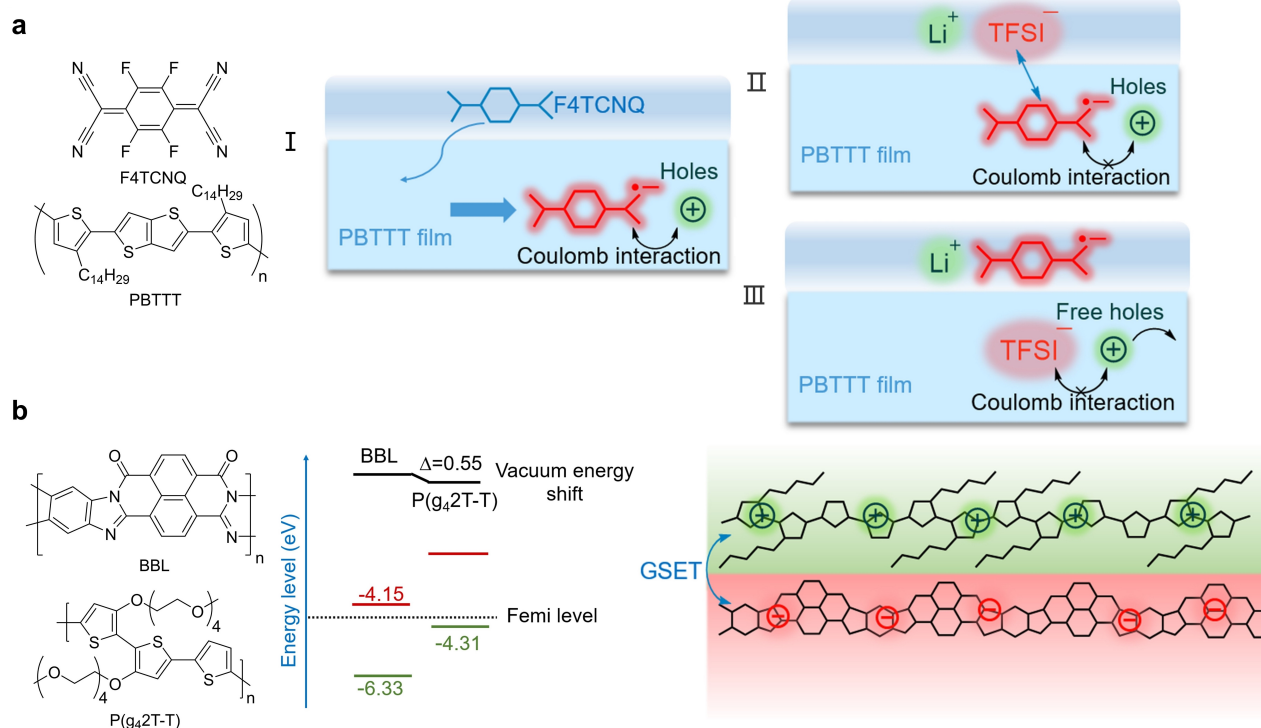


**Figure 5.** a) Schematic illustration of the anion exchange process ( $\text{Li}^+ \text{TFSI}^-$  for example) to enhance the F4TCNQ doping efficiency developed by Watanabe *et al.* The exchange doping contains three steps: (1) conventional F4TCNQ doping process; (2) TFSI<sup>-</sup> anion replacing the F4TCNQ radical anion; (3) reduced Coulombic interactions between holes and the larger TFSI<sup>-</sup> anions. b) Schematic illustration of the vacuum level shift and ground-state electron transfer (GSET) between poly (benzimidazophenanthroline) BBL and P(g<sub>4</sub>2T-T) in the work by Fabiano *et al.*

and anions of the ionic liquid. After TFSI<sup>-</sup> exchange, the polymer exhibits near 100% anion exchange efficiency with 2.4 times higher electrical conductivity. Undoubtedly, anion exchange is a useful way to fulfill the high-efficiency doping process. Moreover, charge transport studies reveal that the conductivity improvement is attributed to both charge carrier concentration and mobility enhancement, where the latter is mainly due to the reduced Coulomb interaction between holes and the larger TFSI<sup>-</sup> anions. This approach breaks the wall of counterion effect and the redox potential limitation by Marcus theory. Considering the generally existed Coulomb interaction of ionized dopants, it is important to modulate the counterion effect for better OTE performance.

If the doping efficiency can achieve 100%, how the counterions effect the electrical conductivity of polymer film? To answer this question, Siringhaus and co-workers explored the potential influential factors by using a similar counterion exchanging method.<sup>[33]</sup> Using PBTTT as the host polymer, they found that at high doping concentrations, the conductivity is poorly correlated with counterion size, but strongly associated with the paracrystalline disorder of the film, which can be strongly influenced by different counterions. This result suggests that the charge carrier-counterion interactions is negligible in the highly doped polymer films, whereas polymer film crystallinity is more important.

#### 2.4. Doping stability

Doping stability can be divided into air stability and operation stability. Usually, air stability can be enhanced by lowering the LUMO energy level of polymers,<sup>[34]</sup> or by using certain kind of encapsulation.<sup>[35]</sup> In the current OTE systems, most of the dopants are small molecules that easily lead to the phase segregation from polymer network under electrical field or after being heated.<sup>[7]</sup> Recently, Fabiano and co-workers<sup>[36]</sup> reported a ground-state charge transfer (GSET) phenomenon in all-polymer donor-acceptor heterojunctions. When a low ionization potential conjugated polymer (P(g<sub>4</sub>2T-T), donor) contact with a polymer with high electron-affinity (BBL, acceptor), GSET can occur at the interface of the two polymers (Figure 5b). Characterization results indicated that the GSET interaction between the two polymers induced the shift of their vacuum level, suggesting that the interfacial D–A heterojunction can be considered as a doping process. Due to the GSET interaction, a quasi-two-dimensional interfacial layer is formed, which creates channels for both hole and electron transport, leading to five or six orders of magnitude higher conductivity than the separated single layers. Traditional doping methods usually use small molecules as the dopants, where small molecules are not stable and movable in the polymer matrix. In this work, polymers are used as the dopant for each other. By blending the donor polymer (P(g<sub>4</sub>2T-T)) with the acceptor polymer (BBL), the polymer system can exhibit p-type or n-type thermoelectric properties under different blending ratios. More importantly, the blended films are very stable with low conductivity loss at elevated temperatures of up to 200 °C even after 20-hour

heating. This work provides a new concept to apply polymer as the dopant to realize highly stable polymer-polymer doping systems.

### 3. Factors influencing Seebeck coefficient

Seebeck coefficient is the open-circuit voltage obtained between the two ends of a material under an applied temperature gradient,  $S = \Delta V / \Delta T$ . The mobile major charge carriers (electrons or holes) in an OTE material thermo-diffuse from the hot side to the cold side to generate the thermal current ( $J_{e/h}$ ) and thermal voltage (Figure 6a).<sup>[37]</sup> From Mott's transport theory,<sup>[38]</sup> the Seebeck coefficient depends on the slope of the density of state (DOS) near the Fermi level,

$$S \propto \left. \frac{d \ln g(E)}{dE} \right|_{E_F} \quad (2)$$

where  $g(E)$  is density of states and  $E_F$  is the Fermi level of OTEs. Usually, the Fermi level will shift according to the doping level and result in different slopes near the  $E_F$ . The slope of the DOS is determined by the DOS shape of an OTE material (Figure 6b). For example, in a pristine polymer film, the polymer packing can influence the electronic coupling between polymer chains and further change the DOS shape. After doping, structural and energetic disorder induced by dopants usually broaden the DOS, reduce the DOS slope, and decrease the Seebeck coefficient. Considering the close relationship between Seebeck coefficient and charge transport properties, Kang and Snyder proposed a model to describe the mechanisms of electronic conduction for conducting polymers.<sup>[39]</sup> They use the following equation to describe the charge transport:

$$\sigma_E(E, T) = \sigma_{E0}(T) \left( \frac{E - E_t}{k_B T} \right)^s \quad (3)$$

where  $\sigma_E(E, T)$  is the conductivity of OTEs functionalized by energy  $E$  and temperature  $T$ , and  $\sigma_{E0}(T)$  is a temperature-dependent but energy-independent parameter, called transport coefficient. In this model, a transport parameter  $s$  is used to describe different transport behavior and related Seebeck coefficient. They found that  $s = 1$  is typically found in crystalline semiconductors and metals (e.g. PEDOT:tosylate), while  $s = 3$  describes most conjugated polymers that have a thermally activated conductivity. Although this model provides a good fit for the Seebeck coefficient and electrical conductivity data in literature, it does not provide a clear structure-property relationship for designing OTE materials. Therefore, further efforts are needed to understand the factors that influence Seebeck coefficient.

#### 3.1. Structural disorder

Structural disorder is the deviation from the idealized polymer crystalline structure, which can be evaluated by paracrystallinity

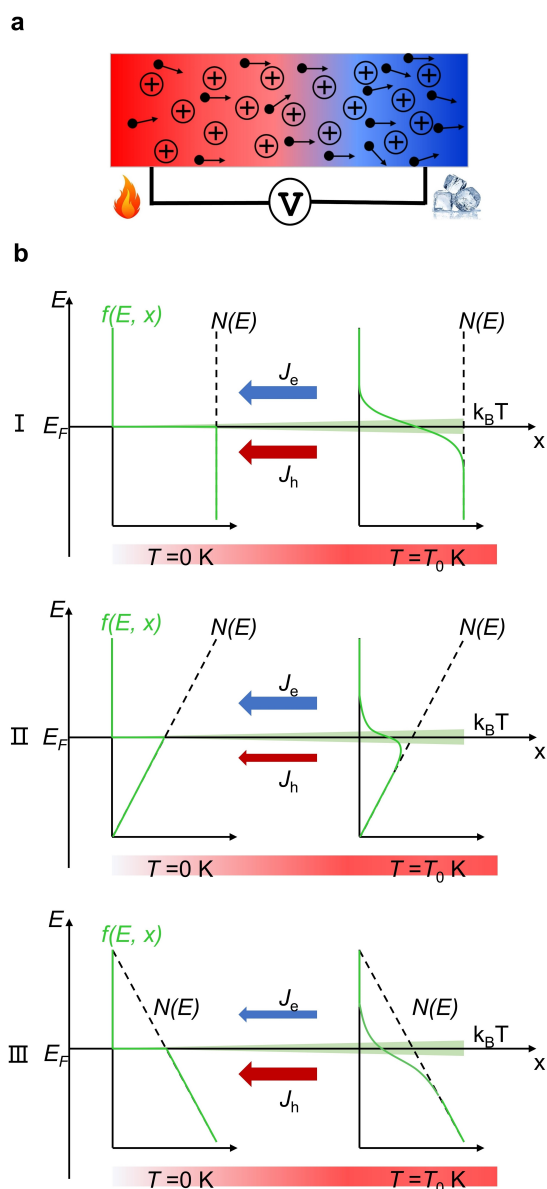


**Figure 6.** a) Schematic illustration of the generation process of the thermal activated hole/electron current which define the Seebeck coefficient. b) Schematic illustration of how the DOS slope near the Fermi level determines the magnitude of the Seebeck coefficient (1) the flat DOS shape generating the equal electron and hole thermal current; (2) the curving DOS shape generating the net electron current and; (3) the net hole current where  $f(E, x)$  is the Fermi-Dirac distribution function and  $N(E)$  is the density of states of OTEs.

(g). This kind of disorder in OTEs changes the electronic coupling between molecules and adds more energetic disorder, which results in localized tail states in DOS of OTEs. Many studies have suggested that the structural disorder, especially positional disorder, will bring energetic disorder and affect the final OTE property. Hippalgaonkar and co-workers<sup>[40]</sup> explained how the paracrystallinity influences charge transport and the Seebeck coefficient. To understand the carrier transport behavior, the authors first built a two-dimensional tight binding model and calculated the DOS width of a large number of P3HT molecules with MD simulation and DFT calculation. They

showed that the paracrystallinity  $g$  indeed correlates with the energetic disorder and the DOS tail. As the  $g$  increasing from 0 to 20%, the DOS tail increase indignantly from 0 to 0.8 eV in P3HT system. Based on the Kang-Snyder model, the authors introduced the scattering parameter ( $r$ ) and the effective DOS ( $N_e/w$ ). The relationship between the Seebeck coefficient and the electrical conductivity is affected by both the scattering parameter  $r$  and the effective DOS. By fitting the literature data of PEDOT, P3HT and PBTTT, they suggested that an ideal OTE material needs high carrier concentration  $N_e$ , narrow DOS width and a proper scattering parameter  $r=1.5$  rather than  $r=-0.5$ . Here, the scattering parameter  $r$  value is consistent with the  $s$  proposed by the Kang-Snyder model ( $s=r+1.5$ ), but the authors provide more structure-property correlations in the study. The authors proposed that building regular three-dimensional molecular packing and effective chain orientation are the key factors to enhance electrical conductivity without sacrificing Seebeck coefficient.

### 3.2. Dopant clustering

In a doped system, unreacted dopants tend to aggregate to form clusters, which undoubtedly brings extra structural and energetic disorder and affects the DOS shape. Venkataraman *et al.*<sup>[41]</sup> found that controlling the size of dopant clusters can modulate the transport parameter  $s$  (Kang-Snyder model) effectively for better OTE performance. The authors employed two polymers P3HT and PDPP4T for verifying the influence of dopant clusters. To exclude the uncertainty of the film morphology damage during doping and de-doping, the authors used iodine vapor to dope the polymers. With the characterization of Kelvin probe force microscopy (KPFM), the authors found that iodine dopant clusters in the PDPP4T film had a smoother spatially distribution under high temperatures and a uniform dopant distribution will lead to narrow energetic disorder with enhanced Seebeck coefficient at the same conductivity. Moreover, the authors found that smaller dopant clusters tend to generate the Gaussian-type DOS distribution rather than the harmful heavy-tailed DOS distribution, which reduces the decrease of Seebeck coefficient. Therefore, the influence of the dopant aggregation cannot be ignored. Modulating the size of dopant clusters and increasing the homogeneity of the film is beneficial to enhance the Seebeck coefficient while maintaining high electrical conductivity.

### 3.3. Polaron or Bipolaron

Compared with inorganic materials, OSCs are structurally "soft". After doping, the backbone structure of an OSC will reorganize to stabilize the positive or negative charge, producing the formation of polarons. The presence of polarons distorts the local molecular structure, shifts the valence and conduction band positions, and creates new energy levels in the bandgap,<sup>[42]</sup> e.g. polymer backbone usually reorganizes from aromatic to quinoid in many cases.<sup>[43]</sup> Further charging a



conjugated polymer leads to the formation of more polarons in one polymer chain, and two polarons may combine to form a bipolaron if the bipolaron is more stable. Polaron and bipolaron can exist simultaneously and both contribute to charge carrier transport. Usually, for a material, the Seebeck coefficient decreases as the conductivity increases. Surprisingly, Crispin and co-workers studied the thermoelectric properties of various PEDOT samples and found that the simultaneous enhancement of the Seebeck coefficient and the electrical conductivity of PEDOT can be achieved after tuning the solid-state molecular packing.<sup>[44]</sup> They observed that through controlling the oxidation level of PEDOT:Tos, the polymer exhibited high electrical conductivities over  $1000 \text{ S cm}^{-1}$  but displayed extremely low EPR signals, indicating the formation of bipolaron species in plenty. Considering these phenomena closely related to the molecular packing orders, they proposed that the discrete energy levels in bipolarons are arranged to form the specific semi-metallic band structure (Figure 7). In particular band structures, their Fermi level located by the side of conduction band and the electron at both sides have an asymmetry arrangement. Hence, the DOS slope of the Fermi level is greatly steeper to produce a higher Seebeck coefficient. The formation of bipolaron in conjugated polymers might benefit the simultaneous enhancement of electrical conductivity and

Seebeck coefficient to achieve higher PF values. Nonetheless, Schwartz *et al.* recently found that PBTDTTP doped with  $\text{F}_4\text{TCNQ}$  exhibits relatively low electrical conductivities ( $1 \times 10^{-3} \text{ S cm}^{-1}$ ) as the stable bipolaronic carriers have a poor mobility and barely contribute to conductivity.<sup>[43]</sup> Thus, the controversy on the bipolaron effects still remains.

#### 4. Summary and outlook

In this review, presenting several representative examples, we have summarized and highlighted several key challenges in the development of OTE materials. According to the parameters that determine  $ZT$  values, the discussions are divided into electrical conductivity and Seebeck coefficient related issues. Note that the influence factors of these two parameters are intertwined. For instance, the miscibility issue in conductivity discussion is clearly correlated with the dopant clustering. The counterion Coulomb interaction with polaron may influence the formation of polaron/bipolaron, and further affect the charge transport and paracrystallinity.<sup>[33]</sup> Therefore, overall consideration of all these interconnected factors is essential during the materials design and device fabrication.

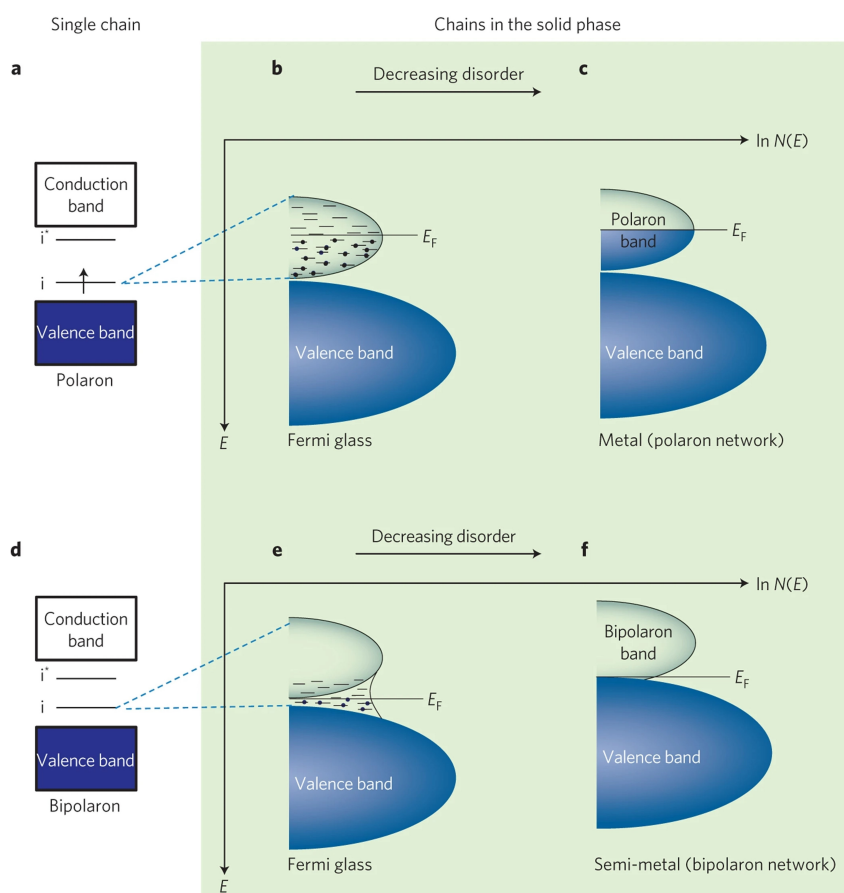


**Figure 7.** Electronic structure of doped conjugated polymer a energy level structure of single polaron and d bipolaron on the polymer chain; The logarithm of the DOS  $\ln N(E)-E$  graph for the polymer Fermi glass solid formed by b polarons and e bipolarons, where  $E_F$  is the Fermi level;  $\ln N(E)-E$  graph for c the metal network of polarons and f the semi-metal network of bipolarons with less disorder. Adapted with permission from Ref. 38. Copyright 2014 Springer Nature.

The past few years have witnessed the thriving of OTE materials in terms of the diversity of their chemical structures, deep understanding of the doping and charge transport mechanisms, and enhancement of device performance. Several OTE materials, including polymers and small molecules, have shown *ZT* values over 0.2 for both p- and n-type materials.<sup>[45]</sup> However, compared with the well-studied inorganic counterparts, the performances of OSC-based TE materials are still lagged far behind, and their doping and charge transport mechanisms are under debate and lack clear guidance for new material design. We consider that future studies need to focus on the following aspects: (1) understanding of the complicated charge transport mechanism of OSCs system with the dopant induced disorder; (2) the development of diverse dopant, doping strategy and new OSCs, especially for n-type materials, since the stability issue of n-type OTE materials is still very challenging; (3) exploring new application scenarios and device integration technologies for OTE materials that can outperform traditional inorganic counterparts, e.g. low-cost and flexible distributed power generation, such as mobile devices, wearable electronics, and sensor networks.

## Acknowledgements

This work is supported by National Natural Science Foundation of China (22075001) and the Beijing Natural Science Foundation (2192020).

## Conflict of Interest

The authors declare no conflict of interest.

**Keywords:** organic thermoelectric materials · conjugated polymers · doping · electrical conductivity · Seebeck coefficient

- [1] J. He, T. M. Tritt, *Science* **2017**, *357*, 9.
- [2] a) G. H. Kim, L. Shao, K. Zhang, K. P. Pipe, *Nat. Mater.* **2013**, *12*, 719–723; b) B. Russ, A. Glaudell, J. J. Urban, M. L. Chabiny, R. A. Segalman, *Nat. Rev. Mater.* **2016**, *1*, 16050.
- [3] G. J. Snyder, E. S. Toberer, *Nat. Mater.* **2008**, *7*, 105–114.
- [4] a) S. Wang, H. Sun, T. Erdmann, G. Wang, D. Fazzi, U. Lappan, Y. Puttison, Z. Chen, M. Berggren, X. Crispin, A. Kiri, B. Voit, T. J. Marks, S. Fabiano, A. Facchetti, *Adv. Mater.* **2018**, *30*, e1801898; b) S. Wang, H. Sun, U. Ail, M. Vagin, P. O. Persson, J. W. Andreasen, W. Thiel, M. Berggren, X. Crispin, D. Fazzi, S. Fabiano, *Adv. Mater.* **2016**, *28*, 10764–10771; c) J. Liu, G. Ye, B. V. Zee, J. Dong, X. Qiu, Y. Liu, G. Portale, R. C. Chiechi, L. J. A. Koster, *Adv. Mater.* **2018**, *30*, e1804290.
- [5] D. Huang, H. Yao, Y. Cui, Y. Zou, F. Zhang, C. Wang, H. Shen, W. Jin, J. Zhu, Y. Diao, W. Xu, C. A. Di, D. Zhu, *J. Am. Chem. Soc.* **2017**, *139*, 13013–13023.
- [6] Y. Shin, M. Massetti, H. Komber, T. Biskup, D. Nava, G. Lanzani, M. Caironi, M. Sommer, *Adv. Electron. Mater.* **2018**, *4*, 1700581.
- [7] a) I. E. Jacobs, A. J. Moule, *Adv. Mater.* **2017**, *29*, 1703063; b) R. Kroon, D. Kiefer, D. Stegerer, L. Yu, M. Sommer, C. Muller, *Adv. Mater.* **2017**, *29*, 1700930.
- [8] Y. Lu, J.-Y. Wang, J. Pei, *Chem. Mater.* **2019**, *31*, 6412–6423.
- [9] K. Broch, D. Venkateshvaran, V. Lemaire, Y. Olivier, D. Beljonne, M. Zelazny, I. Nasrallah, D. J. Harkin, M. Statz, R. D. Pietro, A. J. Kronemeijer, H. Sirringhaus, *Adv. Electron. Mater.* **2017**, *3*, 1700225.
- [10] S. Wang, M. Ha, M. Manno, C. Daniel Frisbie, C. Leighton, *Nat. Commun.* **2012**, *3*, 1210.
- [11] H. Tanaka, K. Kanahashi, N. Takekoshi, H. Mada, H. Ito, Y. Shimoi, H. Ohta, T. Takenobu, *Sci. Adv.* **2020**, *6*, 8.
- [12] a) S. Wang, T. P. Ruoko, G. Wang, S. Riera-Galindo, S. Hultmark, Y. Puttison, F. Moro, H. Yan, W. M. Chen, M. Berggren, C. Muller, S. Fabiano, *ACS Appl. Mater. Interfaces* **2020**, *12*, 53003–53011; b) D. A. Stanfield, Y. Wu, S. H. Tolbert, B. J. Schwartz, *Chem. Mater.* **2021**, *33*, 2343–2356. <https://doi.org/10.1021/acs.chemmater.0c04471>; c) M. T. Fontana, D. A. Stanfield, D. T. Scholes, K. J. Winchell, S. H. Tolbert, B. J. Schwartz, *J. Phys. Chem. C* **2019**, *123*, 22711–22724.
- [13] S. N. Patel, A. M. Glaudell, K. A. Peterson, E. M. Thomas, K. A. O'Hara, E. Lim, M. L. Chabiny, *Sci. Adv.* **2017**, *3*, e1700434.
- [14] V. I. Arkhipov, P. Heremans, E. V. Emelianova, H. Bässler, *Phys. Rev. B* **2005**, *71*, 045214.
- [15] H. Méndez, G. Heimel, S. Winkler, J. Frisch, A. Opitz, K. Sauer, B. Wegner, M. Oehzelt, S. Röthel, S. Duhm, D. Többens, N. Koch, I. Salzmann, *Nat. Commun.* **2015**, *6*, 8560.
- [16] B. Yurash, D. X. Cao, V. V. Brus, D. Leifert, M. Wang, A. Dixon, M. Seifrid, A. E. Mansour, D. Lungwitz, T. Liu, P. J. Santiago, K. R. Graham, N. Koch, G. C. Bazan, T. Q. Nguyen, *Nat. Mater.* **2019**, *18*, 1327–1334.
- [17] C.-Y. Yang, Y.-F. Ding, D. Huang, J. Wang, Z.-F. Yao, C.-X. Huang, Y. Lu, H.-I. Un, F.-D. Zhuang, J.-H. Dou, C.-a. Di, D. Zhu, J.-Y. Wang, T. Lei, J. Pei, *Nat. Commun.* **2020**, *11*, 3292.
- [18] Z. Fan, J. Ouyang, *Adv. Electron. Mater.* **2019**, *5*, 1800769.
- [19] S. N. Patel, A. M. Glaudell, D. Kiefer, M. L. Chabiny, *ACS Macro Lett.* **2016**, *5*, 268–272.
- [20] T. L. D. Tam, J. Xu, *J. Mater. Chem. A* **2021**, *9*, 5149–5163. <https://doi.org/10.1039/d0ta12166e>.
- [21] J. Yang, Z. Zhao, S. Wang, Y. Guo, Y. Liu, *Chem* **2018**, *4*, 2748–2785.
- [22] C. Y. Yang, W. L. Jin, J. Wang, Y. F. Ding, S. Nong, K. Shi, Y. Lu, Y. Z. Dai, F. D. Zhuang, T. Lei, C. A. Di, D. Zhu, J. Y. Wang, J. Pei, *Adv. Mater.* **2018**, *30*, e1802850.
- [23] X. Yan, M. Xiong, J. T. Li, S. Zhang, Z. Ahmad, Y. Lu, Z. Y. Wang, Z. F. Yao, J. Y. Wang, X. Gu, T. Lei, *J. Am. Chem. Soc.* **2019**, *141*, 20215–20221.
- [24] K. Feng, H. Guo, J. Wang, Y. Shi, Z. Wu, M. Su, X. Zhang, J. H. Son, H. Y. Woo, X. Guo, *J. Am. Chem. Soc.* **2021**, *143*, 1539–1552.
- [25] B. D. Naab, S. Guo, S. Olthof, E. G. Evans, P. Wei, G. L. Millhauser, A. Kahn, S. Barlow, S. R. Marder, Z. Bao, *J. Am. Chem. Soc.* **2013**, *135*, 15018–15025.
- [26] J. Liu, G. Ye, H. G. O. Potgieser, M. Koopmans, S. Sami, M. I. Nugraha, D. R. Villalva, H. Sun, J. Dong, X. Yang, X. Qiu, C. Yao, G. Portale, S. Fabiano, T. D. Anthopoulos, D. Baran, R. W. A. Havenith, R. C. Chiechi, L. J. A. Koster, *Adv. Mater.* **2020**, *33*, e2006694.
- [27] E. E. Perry, C.-Y. Chiu, K. Moudgil, R. A. Schlitz, C. J. Takacs, K. A. O'Hara, J. G. Labram, A. M. Glaudell, J. B. Sherman, S. Barlow, C. J. Hawker, S. R. Marder, M. L. Chabiny, *Chem. Mater.* **2017**, *29*, 9742–9750.
- [28] M. Xiong, X. Yan, J. T. Li, S. Zhang, Z. Cao, N. Prine, Y. Lu, J. Y. Wang, X. Gu, T. Lei, *Angew. Chem. Int. Ed.* **2021**, *60*, 8189–8197. <https://doi.org/10.1002/anie.202015216>.
- [29] a) H. Hu, P. C. Y. Chow, G. Zhang, T. Ma, J. Liu, G. Yang, H. Yan, *Acc. Chem. Res.* **2017**, *50*, 2519–2528; b) Z.-F. Yao, Y.-Q. Zheng, Q.-Y. Li, T. Lei, S. Zhang, L. Zou, H.-Y. Liu, J.-H. Dou, Y. Lu, J.-Y. Wang, X. Gu, J. Pei, *Adv. Mater.* **2019**, *31*, 1806747.
- [30] B. Saglio, M. Mura, M. Massetti, F. Scuratti, D. Beretta, X. Jiao, C. R. McNeill, M. Sommer, A. Famulari, G. Lanzani, M. Caironi, C. Bertarelli, *J. Mater. Chem. A* **2018**, *6*, 15294–15302.
- [31] a) R. Q. Png, M. C. Ang, M. H. Teo, K. K. Choo, C. G. Tang, D. Belaineh, L. L. Chua, P. K. Ho, *Nat. Commun.* **2016**, *7*, 11948; b) I. Salzmann, G. Heimel, M. Oehzelt, S. Winkler, N. Koch, *Acc. Chem. Res.* **2016**, *49*, 370–378.
- [32] Y. Yamashita, J. Tsurumi, M. Ohno, R. Fujimoto, S. Kumagai, T. Kurosawa, T. Okamoto, J. Takeya, S. Watanabe, *Nature* **2019**, *572*, 634–638.
- [33] I. E. Jacobs, G. D'Avino, Y. Lin, V. Lemaire, Y. Huang, X. Ren, D. Simatos, W. Wood, C. Chen, T. Harrelson, T. Mustafa, C. A. O'Keefe, L. Spalek, D. Tjhe, M. Statz, L. Lai, P. A. Finn, W. G. Neal, J. Strzalka, C. B. Nielsen, J.-K. Lee, S. Barlow, S. R. Marder, I. McCulloch, S. Fratini, D. Beljonne, H. Sirringhaus, **2021**, p. arXiv:2101.01714.
- [34] D. Nava, Y. Shin, M. Massetti, X. Jiao, T. Biskup, M. S. Jagadeesh, A. Calloni, L. Duo, G. Lanzani, C. R. McNeill, M. Sommer, M. Caironi, *ACS Appl. Mater. Interfaces* **2018**, *1*, 4626–4634.
- [35] Y. Lu, Z. D. Yu, R. Z. Zhang, Z. F. Yao, H. Y. You, L. Jiang, H. I. Un, B. W. Dong, M. Xiong, J. Y. Wang, J. Pei, *Angew. Chem. Int. Ed.* **2019**, *58*, 11390–11394; *Angew. Chem.* **2019**, *131*, 11512–11516.

- [36] K. Xu, H. Sun, T. P. Ruoko, G. Wang, R. Kroon, N. B. Kolhe, Y. Puttison, X. Liu, D. Fazzi, K. Shibata, C. Y. Yang, N. Sun, G. Persson, A. B. Yankovich, E. Olsson, H. Yoshida, W. M. Chen, M. Fahlman, M. Kemerink, S. A. Jenekhe, C. Muller, M. Berggren, S. Fabiano, *Nat. Mater.* **2020**, *19*, 738–744.
- [37] H. Fritzsche, *Solid State Commun.* **1971**, *9*, 1813–1815.
- [38] M. Jonson, G. Mahan, *Phys. Rev. B* **1980**, *21*, 4223.
- [39] S. D. Kang, G. J. Snyder, *Nat. Mater.* **2017**, *16*, 252–257.
- [40] A. Abutaha, P. Kumar, E. Yildirim, W. Shi, S. W. Yang, G. Wu, K. Hippalgaonkar, *Nat. Commun.* **2020**, *11*, 1737.
- [41] C. J. Boyle, M. Upadhyaya, P. Wang, L. A. Renna, M. Lu-Diaz, S. Pyo Jeong, N. Hight-Huf, L. Korugic-Karasz, M. D. Barnes, Z. Aksamija, D. Venkataraman, *Nat. Commun.* **2019**, *10*, 2827.
- [42] a) J. L. Bredas, G. B. Street, *Acc. Chem. Res.* **1985**, *18*, 309–315; b) G. Heimel, *ACS Cent. Sci.* **2016**, *2*, 309–315.
- [43] M. G. Voss, J. R. Challa, D. T. Scholes, P. Y. Yee, E. C. Wu, X. Liu, S. J. Park, O. Leon Ruiz, S. Subramanian, M. Chen, S. A. Jenekhe, X. Wang, S. H. Tolbert, B. J. Schwartz, *Adv. Mater.* **2020**, *33*, 2000228.
- [44] O. Bubnova, Z. U. Khan, H. Wang, S. Braun, D. R. Evans, M. Fabretto, P. Hojati-Talemi, D. Dagnelund, J. B. Arlin, Y. H. Geerts, S. Desbief, D. W. Breiby, J. W. Andreasen, R. Lazzaroni, W. M. Chen, I. Zozoulenko, M. Fahlman, P. J. Murphy, M. Berggren, X. Crispin, *Nat. Mater.* **2014**, *13*, 190–194.
- [45] a) J. Ding, Z. Liu, W. Zhao, W. Jin, L. Xiang, Z. Wang, Y. Zeng, Y. Zou, F. Zhang, Y. Yi, Y. Diao, C. R. McNeill, C.-a. Di, D. Zhang, D. Zhu, *Angew. Chem. Int. Ed.* **2019**, *58*, 18994–18999; *Angew. Chem.* **2019**, *131*, 19170–19175; b) J. Liu, B. van der Zee, R. Alessandri, S. Sami, J. Dong, M. I. Nugraha, A. J. Barker, S. Rousseva, L. Qiu, X. Qiu, N. Klasen, R. C. Chiechi, D. Baran, M. Caironi, T. D. Anthopoulos, G. Portale, R. W. A. Havenith, S. J. Marrink, J. C. Hummelen, L. J. A. Koster, *Nat. Commun.* **2020**, *11*, 5694.

---

Manuscript received: March 20, 2021  
 Revised manuscript received: April 26, 2021  
 Accepted manuscript online: April 29, 2021  
 Version of record online: May 13, 2021